ARTICLE

Drosophila Atg9 regulates the actin cytoskeleton via interactions with profilin and Ena

Viktória Kiss[1,2] · András Jipa [1,2] · Kata Varga[1] · Szabolcs Takáts[3,4] · Tamás Maruzs[1] · Péter Lőrincz[3,4] ·
Zsófia Simon-Vecsei[3] · Szilárd Szikora[1] · István Földi[1] · Csaba Bajusz[1,2] · Dávid Tóth[1] · Péter Vilmos[1] · Imre Gáspár[5] ·
Paolo Ronchi[6] · József Mihály[1] · Gábor Juhász [1,3]

Abstract

Autophagy ensures the turnover of cytoplasm and requires the coordinated action of Atg proteins, some of which also have moonlighting functions in higher eukaryotes. Here we show that the transmembrane protein Atg9 is required for female fertility, and its loss leads to defects in actin cytoskeleton organization in the ovary and enhances filopodia formation in neurons in *Drosophila*. Atg9 localizes to the plasma membrane anchor points of actin cables and is also important for the integrity of the cortical actin network. Of note, such phenotypes are not seen in other Atg mutants, suggesting these are independent of autophagy defects. Mechanistically, we identify the known actin regulators profilin and Ena/VASP as novel binding partners of Atg9 based on microscopy, biochemical, and genetic interactions. Accordingly, the localization of both profilin and Ena depends on Atg9. Taken together, our data identify a new and unexpected role for Atg9 in actin cytoskeleton regulation.

Introduction

The cellular self-degradative pathway known as autophagy plays crucial roles in a variety of physiological and

✉ Gábor Juhász
szmrt@elte.hu

1 Institute of Genetics, Biological Research Centre, Hungarian Academy of Sciences, Szeged, Hungary

2 Doctoral School of Biology, University of Szeged, Szeged, Hungary

3 Department of Anatomy, Cell and Developmental Biology, Eötvös Loránd University, Budapest, Hungary

4 Premium Postdoctoral Program, Hungarian Academy of Sciences, Szeged, Hungary

5 Developmental Biology Unit, European Molecular Biology Laboratory, Heidelberg, Germany

6 Electron Microscopy Core Facility, European Molecular Biology Laboratory, Heidelberg, Germany

pathological processes, including differentiation, development, aging, neurodegeneration, and tumorigenesis [1, 2]. Atg9 is the only known evolutionarily conserved transmembrane protein among *Atg* gene products and is likely responsible for membrane transport and recycling of membranes during autophagosome biogenesis [3]. Mammalian ATG9 (mATG9) proteins localize to the trans-Golgi network, endosomal system, and plasma membrane under normal conditions, translocating to autophagic membranes upon induction of autophagy [4, 5].

Autophagy was suggested to be involved in oogenesis in *Drosophila*, potentially by affecting the communication between somatic and germline cells in the ovary, because the knockdown or mutation of various Atg genes in somatic follicle cells interfered with proper development of oocytes in mosaic animals [6, 7]. Interestingly, oogenesis could still proceed when both follicle cells and germline cells were mutant for Atg1 or Atg7. However, unlike other viable Atg null mutants including Atg3/Aut1, Atg5, Atg7, and Atg16 [8, 9], Atg9 knock-out female flies are almost completely female sterile (this study, and ref. [10]), raising the possibility that Atg9 plays an autophagy-independent role in oocyte development.

During oogenesis, nurse cells (NCs) contract to expel their cytoplasmic contents into the oocyte (a process called

dumping) through so-called ring canals: actin-rich arrested cleavage furrows [11]. Just before dumping, parallel actin cables extending from the plasma membrane to the nucleus assemble in the cytoplasm of NCs, with the (+) ends of actin cables situated in small plasma membrane protrusions that are similar to filopodia, microvilli, bristles, and stereocilia [12]. Actin filaments are asymmetric polymers that extend by monomer addition at their (+) end (also known as barbed end). Capping proteins bind barbed ends to prevent further addition of actin monomers [13]. The action of capping proteins is antagonized by the tip complex subunit Enabled (Ena, the *Drosophila* homolog of VASP, vasodilator-stimulated phosphoprotein) that promotes continued polymerization at the barbed end [14]. In addition, Ena/VASP can bundle actin filaments in the actin-rich protrusions [15], and it can tether the complex consisting of an actin monomer and profilin, which provides monomers for actin polymerization at the tip [16].

In this study, we generated a null mutant for *Drosophila* Atg9 and found that apart from the expected autophagy defect, loss of Atg9 function also caused female sterility and aberrant actin network organization in NCs. Furthermore, ablation of Atg9 enhanced filopodial growth in primary embryonic neurons, suggesting a general actin-cytoskeleton regulator function for Atg9. Mechanistically, we have identified Ena/VASP and profilin as novel interacting partners of Atg9, pointing to an autophagy-independent role of Atg9 in actin organization.

Materials and methods

Drosophila maintenance and stocks

Flies were raised on standard yeast/cornmeal agar at 25 °C unless otherwise noted. Three to five days old females were used for all experiments. The following *Drosophila* strains were used: $Atg9^{B5}$, $Atg9^{B5}$; $3xHA$-$Atg9$, $Atg9^{B5}$; $Atg9$–$3xmCherry$, $Df(2 R)ED2487$, $slbo$-$Lifeact$-GFP (all described in this study), ena^{23}, $chic^{221}$, nos-$Gal4$, tub-$Gal4$ (obtained from the Bloomington Stock Center), tub-GFP-$p62$, genomic promoter-driven $3xmCherry$-$Atg8a$, $Atg5^{5CC5}$ and previously described stocks for generation of mosaic animals [17]. Double mutant lines containing the $Atg9^{B5}$ allele and the $chic^{221}$ or ena^{23} alleles were generated using standard genetic crosses and recombinations.

Generation of Atg9-3xHA and -3xmCherry constructs

For the generation of genomic promoter-driven Atg9–3xHA rescue transgene, using genomic fly DNA we PCR

amplified a 3153 bp region containing the Atg9 gene and its promoter using genomic fly DNA and primers 3′-GCGGCCGCGGCGCGCCTGCCGCCATACAGCT CACTCC-5′ and 5′-GCGGCCGCATGGCGCGCCTGAG CGGATGCTACCCAAAAGC-3′, and cloned it into pGen-3xHA vector as an AscI fragment. In this construct, the stop codons were replaced by 3xHA coding sequences [18]. Atg9 sequences from the gen-3xHA-Atg9 vector were moved into our gen-3xmCherry vector [19] to generate gen-Atg9-3xmCherry. Transgenic lines were established by Bestgene.

Antibodies

Primary antibodies used in this study were rat anti-Atg9 (WB 1:300) [20], rat anti-HA (IF 1:150, WB 1:1500, Roche, 11867431001), mouse anti-tubulin (1:2000, DSHB, AA12.1), mouse anti-Ena (IF/WB 1:40, DSHB, 5G2), mouse anti-Profilin (IF 1:10, DSHB, chi1J), rat anti-DE-cadherin (IF 1:10, DSHB, DCAD2) rat anti-actin (WB 1:5000, Babraham Technix, BT-GB-237P), mouse anti-Flag M5 (WB 1:1000, Sigma, F4042), mouse anti-Fasciclin II antibody (1:500, DSHB, 1D4). The following secondary antibodies were used: goat anti-mouse Alexa Fluor 488 (A-11001), goat anti-mouse Alexa Fluor 546 (A-11003), goat anti-mouse Alexa Fluor 660 (A-21055), goat anti-rabbit Alexa Fluor 488 (A-11008), goat anti-rabbit Alexa Fluor 546 (A-11010), goat anti-rabbit Alexa Fluor 660 (A-21074), goat anti-rat Alexa Fluor 488 (A-11006), goat anti-rat Alexa Fluor 546 (A-11081)—all purchased from Invitrogen and biotinylated goat anti-mouse antibody (1:500, Jackson, 115-065-003). For immunoprecipitation assays, monoclonal mouse anti-HA conjugated agarose beads (Sigma, A2095) and mouse monoclonal anti-FLAG M2 conjugated Magnetic Beads (Sigma, M8823) were used.

Generation of Atg9 mutants

The Atg9[B5] allele was generated by CRISPR/Cas9 mediated genome editing using a double gRNA approach as before [21]. The gRNA sequences were cloned into pCFD4 [22] using Gibson Assembly Master Mix (New England Biolabs) following BbsI digestion, using the oligonucleotides:

Atg9_1: 5′-TATATAGGAAAGATATCCGGGTGAAC TTCGTGAGGTAATCACGGTATGGCGTTTTAGAGC TAGAAATAGCAAG-3′

Atg9_2: 5′-ATTTTAACTTGCTATTTCTAGCTCTA AAACCATATCAACTACCGCTCCCTCGACGTTAAAT TGAAAATAGGTC-3′

Viable candidate Atg9 mutant flies were crossed to *Df(2 R)ED2487* deficiency and hemizygotes were analyzed by western blot for accumulation of the selective autophagy cargo Ref(2)P/p62, followed by PCR screening and

sequencing. The *Atg9^{B5}* allele carries a 2464 bp deletion in the right arm of the second chromosome.

For generation of MARCM somatic mutant fat body clones the *Atg9^{B5}* mutation was first recombined onto an *FRT42B* containing chromosome, and then this line was crossed with *hsFlp; QUAS-Tomato FRT42B; ET49-QF, tub-QS* or *hsFlp; QUAS-mCD8-GFP FRT42B; ET49-QF, tub-QS*. Progeny (2–4 h embryos) was heat shocked in 37 °C water bath for 1 h. The larvae were kept at 25 °C for 3 days and starved in 20% sucrose solution for 3 h before dissection.

Y2H assay

Coding sequences of CTD1 (1–351 bp), CTD2 (580–1002 bp), and C-terminal cytosolic domain (CTD4; 1618–2538 bp) cytosolic domains of Atg9 from UAS-GFP-Atg9 vector, profilin from the EST LD15851 (DGRC), Actin5C from the EST RE02927 (DGRC), and Ena/VASP from LD23655 (DGRC) were PCR amplified. The Atg9 fragments were cloned into pGADT7 and Actin 5C, Profilin, and Ena coding sequences were cloned to pGBKT7 vectors, respectively, and then transformed into AH190 yeast cells as described previously [19]. Synthetic Defined (SD) Medium was used with supplement amino acids, as noted in the experiments. To destroy the poly-Pro binding region of profilin we changed Trp3 to Ala using the following primers: ATATGAATTCATGAGCGCGCAAGA TTATGTGGACAACCAACTC; ATATGTCGACACTAG TACCCGCAAGTAATCAGATAATCTCC. The PCR product was cloned into GBKT7 vector. For further yeast two hybrid analysis, the coding region of Ena/VASP was subcloned to pGADT7 vector as well.

GST pull down tests

GST-profilin was generated by cloning sequences coding for full-length profilin into pETARA vector and purified along with GST as negative control. These recombinant proteins were immobilized to Glutathione Sepharose beads (GE Life Sciences, 17075604), blocked in 5% BSA, incubated with Atg9–3xHA expressing female *Drosophila* lysate. Lastly, protein samples were analyzed by western blot using anti-HA antibody.

Generation of plasmids for S2R+ cell experiments

Five different pUAS vectors were generated. pUASp-GFP-Atg9 was generated by PCR amplification of the Atg9 gene from genomic fly DNA using oligos with BglII and XbaI sites and then it was inserted into BglII and XbaI digested pUASp-GFP vector, where an XhoI site was next to the XbaI site in distal position. Next the Atg9 C-terminus

coding sequence (1618–2538 bp) was amplified from the pUASp-GFP-Atg9 vector using oligos with BglII and XhoI sites and was inserted into BglII–XhoI digested pUASp-GFP-Atg9 vector resulting in pUASp-GFP-Atg9C. As the source of the 56 aa long KASH domain we amplified the KASH domain sequence of Msp300 from 13481 to 13540 bp using oligos with BglII and XhoI sites. The end of Atg9 C-terminus was amplified using oligos with SpeI and XhoI sites for removing the last UAG stop codon of Atg9, then it was inserted into SpeI–XhoI cut pUASp-GFP-Atg9 and pUASp-GFP-Atg9C vectors. The KASH domain coding sequence was inserted into BglII–XhoI digested pUASp-GFP and XhoI digested pUASp-GFP-Atg9-nostop and pUASp-GFP-Atg9C-nostop resulting in pUASp-GFP-KASH, pUASp-GFP-Atg9-KASH, and pUASp-GFP-Atg9C-KASH plasmids, respectively.

S2R+ cell maintenance and transfection

The S2R+ *Drosophila* cell line (obtained from the Drosophila Genomics Resource Center) was maintained in Schneider's *Drosophila* medium (Lonza) complemented with 10% Fetal Bovine Serum (Biowest) and 1% antibiotics (Penicillin-Streptomycin, Lonza) at 25 °C. On the 2nd day after transfection of UAS plasmids and MT-Gal4 using Effectene (Qiagen) in 1.8×10^5 cells/well in 24-well plates, cells were incubated overnight with $CuSO_4$ (1 mM final concentration) to trigger protein expression.

Primary embryonic neural cell culture and immunofluorescence

Whole, dechorionated embryos were squashed in Schneider's medium supplemented with 20% heat-inactivated FBS, 2 µg/mL insulin and penicillin-streptomycin solution (Lonza). Embryonic homogenates were centrifuged at $380 \times g$ for 4 min at room temperature. Pellets were re-suspended in complete medium and the cells were grown at 27 °C on glass coverslips or in glass-bottom Petri dishes for live imaging (MatTek). Cultured neuron samples were fixed at 6 h in vitro (HIV). Samples were initially fixed and extracted for 1 min using a solution of 0.3% (v/v) glutaraldehyde and 0.25% (v/v) Triton X-100 in cytoskeleton buffer (CB, 10 mM PIPES, pH 7, 150 mM NaCl, 5 mM EGTA, 5 mM glucose, and 5 mM $MgCl_2$), and then post-fixed for 15 min in 2% (v/v) glutaraldehyde in CB. The samples were briefly washed in CB, then permeabilized and blocked in blocking buffer (5% w/v goat serum, 0.2% v/v Triton X-100 in CB) for 30 min. Samples were stained with the antibodies indicated above. The samples were mounted in anti-fade reagent (ProLong Gold, Life technologies, P36930) for imaging.

Immunostaining of embryonic CNS and ovaries

Immunostaining of embryonic ventral nerve cords was carried out as described [23]. Briefly, stage 16–17 fixed embryos were incubated with anti-Fasciclin II antibody and then with biotinylated goat anti-mouse antibody followed by DAB (Sigma) immune-detection using Vectastain ABC kit (Vector Laboratories, SK-6604).

Ovaries were dissected in PBS and fixed in 4% formaldehyde (in PBS) for 20 min at room temperature. After fixation, samples were washed in PBT (PBS containing 0,5% Triton X-100) for 10 min three times, then blocked in PBT containing 1% BSA + 5% FCS for 1 h. The samples were incubated with the primary antibodies in PBT-BSA-FCS at 4 °C for overnight. On the following day, ovaries were washed with PBT and incubated with fluorescently labeled secondary antibodies at room temperature for 1 h and immediately incubated with DAPI in PBS for 15 min. F-actin was stained using fluorescently labeled phalloidin: Alexa Fluor 488 Phalloidin (Invitrogen, A12379) Alexa Fluor 546 Phalloidin (Invitrogen, A22283). Samples were mounted in Vectashield Antifade Mounting Medium (VECTOR Laboratories, H-1000).

For colocalication assays, salivary glands of L3 wandering larvae were dissected in ice cold PBS and fixed using 4% FA in PBS for 30 min at RT. Incubation with anti-FLAG antibody (1:200) was performed at 4 °C overnight, incubation with the secondary antibody was performed at RT for 1 h. Permeabilization, washing, and blocking steps were carried out at RT following standard protocols.

Confocal microscopy

S2 cells adhered to round glass coverslips were fixed in 4% PFA-PBS, immunostained and mounted in Fluoromount G (Thermo Fisher Scientific, 00-4958-02) then imaged with a Leica TCS SP5 confocal microscope using a 63.0 × 1.40 oil objective.

For Lysotracker staining, *Drosophila* larval fat bodies were dissected larvae starved for 4 h, incubated in 100 μM Lysotracker Red (Invitrogen, L7528) for 5 min with DAPI (Invitrogen, D1306) was used. In PBS, mounted in PBS:Glycerol (1:1 mixture), immediately followed by imaging.

Lower magnification fat tissue, CNS, and egg chamber images were acquired using a Zeiss AxioImager M2 microscope equipped with an ApoTome 2 grid confocal module and an ORCA-Flash4.0 LT sCMOS camera (Hamamatsu). To acquire higher magnification images, a Leica SP5 microscope was used in the case of *Drosophila* S2 cells, and a Zeiss LSM800 microscope was used for visualizing actin cable network in egg chambers.

## Correlative fluorescence microscopy and electron tomography

For studying Atg9-3xmCherry localization on the ultrastructural level, 10–15 ovaries of 3 days old females were embedded into lowicryl resin using high-pressure freezing, freeze-substitution and embedding for 3D Correlative Light and Electron Microscopy (CLEM). This experiment was carried out in the Electron Microscopy Core Facility of European Molecular Biology Laboratory, Heidelberg, following a recently developed method [24].

Statistics

All experiments were repeated at least once and data from at least nine individual animals/genotype were evaluated. All data points were always included in the analyses. In primary embryonic neural cell assays, cells were randomly selected from slides containing mutant or control primary embryonic neurons. In these cases, only cells with their axons and filopodia in the focal plane were selected to ensure that the full-length axons and all filopodia were included in quantifications. For border cell migration analysis, images of border cell clusters were captured at multiple focal planes to ensure that all cells were included in the analysis.

The quantified data were evaluated using GraphPad Prism 5 or SPSS 21 (IBM) as before [25, 26]. Different genotypes were always evaluated using the same settings and randomly taken images. The evaluator was always unaware of the identity of experimental groups during statistical analysis. Variance analysis was always carried out using SPSS or GraphPad prior to the actual comparisons of datasets. The variance was similar between the compared groups, except when U or Kruskal–Wallis tests were used. Two-tailed, two-sample unpaired t-test was used for comparing two samples that showed normal distribution (Figs. 8c, S6d, and S3c). Kruskal–Wallis test was used for comparing multiple samples where at least one did not show normal distribution of data (Figs. 3a, 4d, e, and Fig. S1c). In one case Mann–Whitney U test was used for comparing two datasets as one experimental group did not show normal distribution of data (Fig. S3d). Fisher's exact test was used for analysing Figs. 3b and S2b. [27]

Error bars denote ± SEM in bar charts. In the box plots (Fig. S3c, d), bars (blue and yellow) show the data ranging between the upper and lower quartiles; median is indicated as a horizontal black line and mean is indicated by 'x' within boxes. Exact n numbers and p values are included in figure legends for all experiments and genotypes (note that in Kruskal–Wallis tests, the SPSS software does not give the exact value if it is under 0.001).
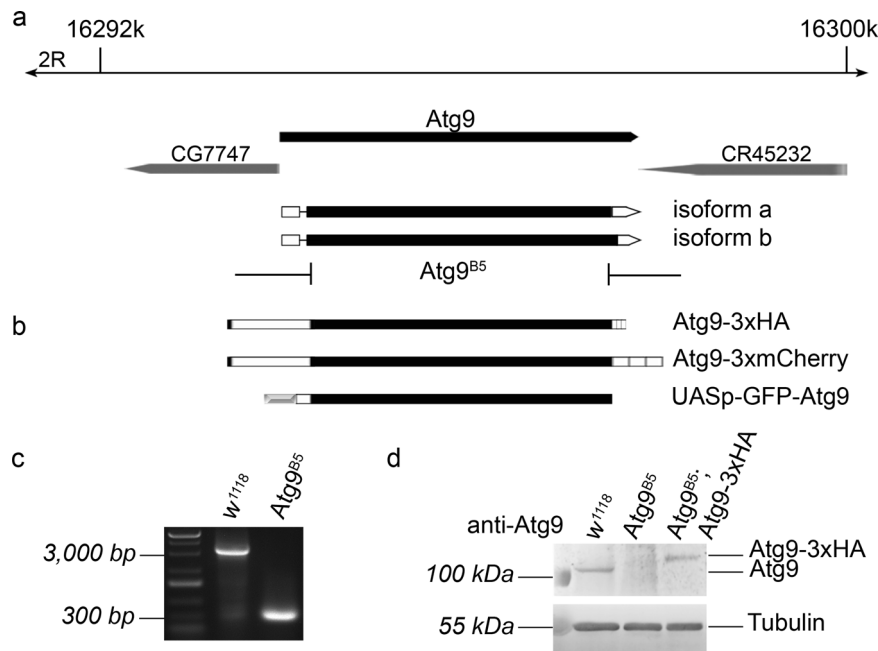
Fig. 1 Generation of an Atg9 null allele and Atg9 transgenes. The $Atg9^{B5}$ allele was generated using CRISPR/Cas9 and removes almost the entire protein coding sequence of the *Drosophila* Atg9 gene (**a**). Two Atg9 transgenes driven by Atg9 promoter sequences were generated, which encode C-terminal fusion proteins to either 3xHA or 3xmCherry (**b**). Furthermore, an UAS-GFP-Atg9 plasmid was generated for transfection into macrophage-like *Drosophila* S2 cells (**b**). Atg9 deletion was confirmed by PCR on genomic DNA samples (**c**). The lack of endogenous Atg9 protein expression in $Atg9^{B5}$ mutants, and the presence of Atg9-3xHA in genetically rescued flies were detected in immunoblot (**d**) using our anti-Atg9 antibody

Results

Generation and characterization of *Atg9* mutant flies

We generated *Atg9* mutants using the CRISPR/Cas9 system to obtain the $Atg9^{B5}$ allele that removes most of the protein coding sequence starting from amino acid 5 (out of 845), and also creates a frameshift producing a stop at the 6th codon in the mutant (Fig. 1a). The 2464 bp deletion could be readily detected in mutants using PCR (Fig. 1c). We compared Atg9 expression in wild type and mutant adult females, which confirmed the lack of endogenous Atg9 protein in the mutants in western blots (Fig. 1d). Atg9 expression in mutants was restored by a genomic *Atg9* promoter-driven Atg9 transgene tagged by 3xHA at its C-terminus (Fig. 1b, d, note that we used a C-terminally 3xmCherry-tagged version of this reporter/rescue transgene for microscopy). These results showed that the $Atg9^{B5}$ mutation is a null allele.

Homozygous $Atg9^{B5}$ and hemizygous $Atg9^{B5}/Df(2R)$ *ED2487* flies are morphologically normal but semi-lethal that could be rescued by our genomic promoter-driven transgenes, in line with the known phenotype of previously described *Atg* mutants [9, 10, 21]. RNAi knockdown studies revealed that Atg9 has a crucial role in autophagy [28, 29]. To confirm that our *Atg9* null mutation also inhibits this process we carried out mosaic analysis. We generated clone cells homozygous for the $Atg9^{B5}$ mutation in larval fat tissue. As expected, starvation-induced punctate autolysosomal Lysotracker Red staining that is widely used to assess autophagy in *Drosophila* fat cells was absent in *Atg9* mutant cells (Fig. 2a). A more specific marker for autophagic structures is mCherry-Atg8a, as Atg8a is anchored into the membrane of phagophores and autophagosomes, and mCherry remains fluorescent after delivery to autolysosomes. Again, punctate 3xmCherry-Atg8a signal was absent from mutant cells compared with neighboring control cells in starved animals (Fig. 2b). Impaired autophagy is known to trigger accumulation of p62/Ref(2)P, the selective receptor for ubiquitinated proteins that is turned over by autophagy. Indeed, GFP-p62 (driven by the constitutive tubulin promoter) aggregates were readily detected in *Atg9* mutant clone cells compared with the control cells in well-fed larvae (Fig. 2c). The increased protein level of endogenous p62 was also obvious in western blots of *Atg9* null mutant flies compared with control or genetically rescued mutant animals using either of our two transgenes expressed from the genomic *Atg9* promoter in all tissues (Fig. 2d). Thus, both selective and starvation-induced bulk autophagy are impaired in our *Atg9* null mutant flies.
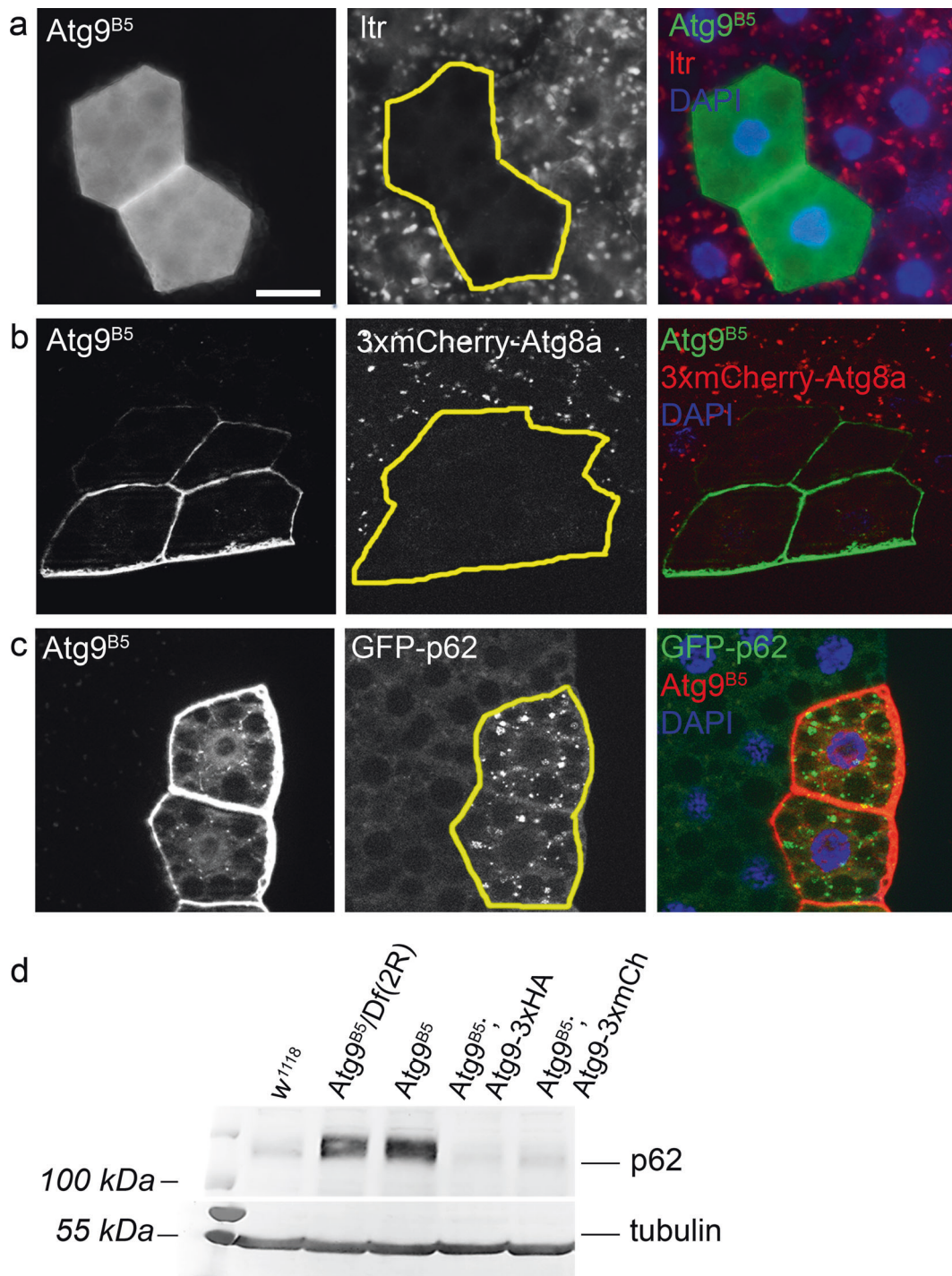
Fig. 2 Atg9 is necessary for starvation-induced and basal autophagy. *Atg9^B5* null mutant larval fat cells are marked by GFP (green, **a** and **b**) or mTomato (red, **c**) expression in mosaic animals. The formation of starvation-induced lysotracker-positive autolysosomes (**a**) and 3xmCherry-Atg8a positive autophagic structures (**b**) is inhibited in mutant cells compared with the surrounding control cells. *Atg9^B5* null mutant cells in well-fed animals show prominent accumulation of constitutive tubulin-promoter driven GFP-p62 aggregates (**c**). In line with this, western blot from adult fly lysates shows increased endogenous p62 level in case of both *Atg9* null mutants and hemizygotes. (**d**). Expression of either Atg9-3xHA or Atg9-3xmCherry (Atg9-3xmCh) restores normal p62 levels in mutants (**d**). Scale bar (**a**) represents 20 µm for **a**–**c**
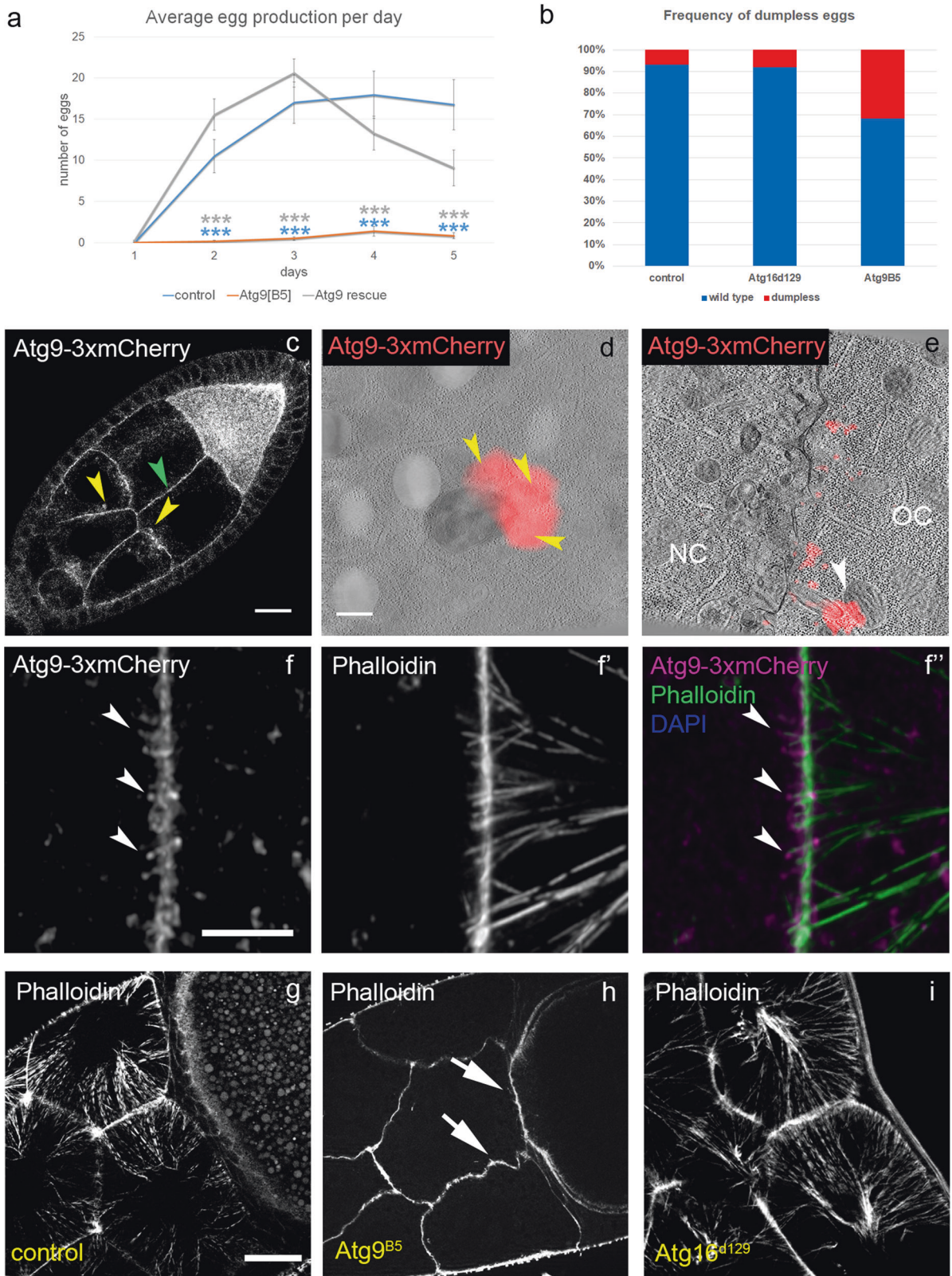
◀ **Fig. 3** Atg9 is required for female fertility. Homozygous *Atg9*[B5] mutant female flies produce much fewer eggs compared with controls or mutants rescued with the Atg9–3xHA transgene based on Kruskal–Wallis test, $n = 20$/genotype, ***$p < 0.001$. **a** The frequency of dumpless eggs is significantly higher among the eggs laid by *Atg9*[B5] mutant females compared with wild type and *Atg16*[d129] controls. Note that females bearing *Atg9*[B5] germline clones produce dumpless eggs with a similar frequency as the Atg9[B5] null females (**b**), $p = 0.794$ (*wt-Atg16*), $p = 0.0000084$ (*wt-Atg9*), $p = 0.00005$ (*Atg16-Atg9*) based on Fisher's exact test. In Drosophila egg chambers, Atg9 localizes to punctate structures in the cytoplasm and to the plasma membrane (yellow and green arrowheads), respectively (**c**). CLEM analysis revealed that Atg9 positive structures represent small vesicles (arrowheads) near lysosomes (**d**) and that Atg9 is enriched in actin cable-containing protrusions (white arrowhead) between germline cells (**e**). Phalloidin staining also confirmed the presence of Atg9-3xmCherry at the tip of actin cables (arrowheads) near the plasma membrane, which likely represent actin-rich protrusions (**f**). In stage 10B egg chambers, loss of Atg9 function delays actin cable network formation in nurse cells (arrows point to small initial cables), compared with the fan-shaped bundle pattern in similarly staged control flies and in female fertile homozygous Atg16[d129] autophagy mutants (**g–i**). Scale bar represents 20 μm in **c**, 150 nm in **d** and **e**, 5 μm in **f**, and 20 μm in **g**. NC nurse cell, OC oocyte

Atg9 promotes female fertility independent of autophagy

Despite the viability of our mutants, it was impossible to maintain them as a homozygous stock. The short lifespan, locomotor defect and increased stress sensitivity of Atg9 null mutants have been described [10]. Atg9 mutant males were perfectly fertile when mated with control females, but strikingly, *Atg9* mutant females produced few or no eggs when mated to wild type males, suggesting that this protein is specifically required for female fertility (Fig. 3a). While the ovary of mutant females appears similar to controls in size and shape, most eggs are retained instead of being laid. Of the rarely deposited eggs more than one third are smaller (Figs. 3b and S1a) than wild type eggs, which is often referred to as a "dumpless" phenotype, resulting from impaired dumping of NC cytoplasm into the oocyte. Moreover, persisting NC nuclei are seen in stage 14 egg chambers (Fig. S1b) and cytoplasmic streaming is reduced in *Atg9* but not in *Atg16* mutant oocytes, respectively (Fig. S1c), also indicating a dumping defect.

We next determined the localization of Atg9 in the ovary. Endogenous promoter-driven Atg9-3xmCherry was detected in plasma membranes and internal vesicles in NCs and showed enrichment in the developing oocyte (Fig. 3c). Using CLEM, Atg9-3xmCherry localization was analyzed in detail in stage 10B egg chambers. In the electron microscope, mCherry-positive small vesicles were often associated with lysosomes (Fig. 3d), and Atg9 preferably localized to highly curved plasma membrane regions surrounding actin protrusions between GCs (Fig. 3e). This was also obvious in confocal microscopy: Atg9 accumulated at

the attachment of the actin cables and plasma membrane in filopodia-like protrusions (Fig. 3f). These data suggest that Atg9 preferably resides in highly curved membranes such as small vesicles and filopodia-like structures between GCs.

Based on the presence of Atg9 in filopodia-like actin rich protrusions, we next visualized the actin network in stage 10B egg chambers, at the time when the excessive dumping of NC cytoplasm into the oocyte begins. Compared with wild type and *Atg16*[d129] controls (Fig. 3g, i, the latter one causing defective autophagy with females remaining fertile [8]), fewer and shorter actin cables are usually seen in *Atg9* null mutant NCs at this stage of oogenesis (Fig. 3h, see also Fig. 7a for a slightly later stage). These observations suggest that Atg9 is presumably involved in actin cable network formation in an autophagy-independent manner.

In addition to the germ line, somatic follicle cells also have important roles in oogenesis, including follicular epithelium-derived migrating border cells (BCs). The BC cluster consisting of 6–10 cells migrate collectively from the anterior pole of the egg chamber to the anterior border of the oocyte carrying the polar cells (Fig. S2b) that are responsible for providing signals during embryogenesis. BCs also contribute to eggshell development by forming a specialized structure, the micropyle (note that during fertilization the sperm enters through a hole in the micropyle). BCs reach the anterior border at stage 10 A of oogenesis, and defects in this process lead to female sterility. During migration, BCs show dynamic actin cytoskeleton rearrangement by forming actin rich lamellipodia [30]. Forty-three percent of Atg9 mutant egg chambers show defective BC migration: the most frequent defect (28%) is the disrupted cluster, with one or more migrating border cell separating from the cluster (Fig. S2a). In 15% of mutant egg chambers, cluster integrity is preserved but they fail to reach the oocyte by stage 10. Since these border cell defects may also contribute to the sterility of Atg9 mutant females, we generated mosaic animals with germline clones lacking Atg9. The percentage of dumpless eggs laid by these females was similar to that of full Atg9 mutants (Fig. 3b), suggesting that Atg9 function in the germline is important for female fertility.

Atg9 cooperates with Ena/VASP and profilin to control the actin cytoskeleton in germ cells

The actin cable tip complex protein Ena/VASP localizes to the tip of the filopodia-like actin cables at the plasma membrane [31], similar to what we saw in case of Atg9. Ena forms a constitutive homotetramer with anticapping activity, binds to profilin and F- and G-actin, and bundles actin filaments. To determine whether there is a connection between Ena, profilin and Atg9, we carried out genetic interaction tests. The homozygous *Atg9*[B5] mutation caused
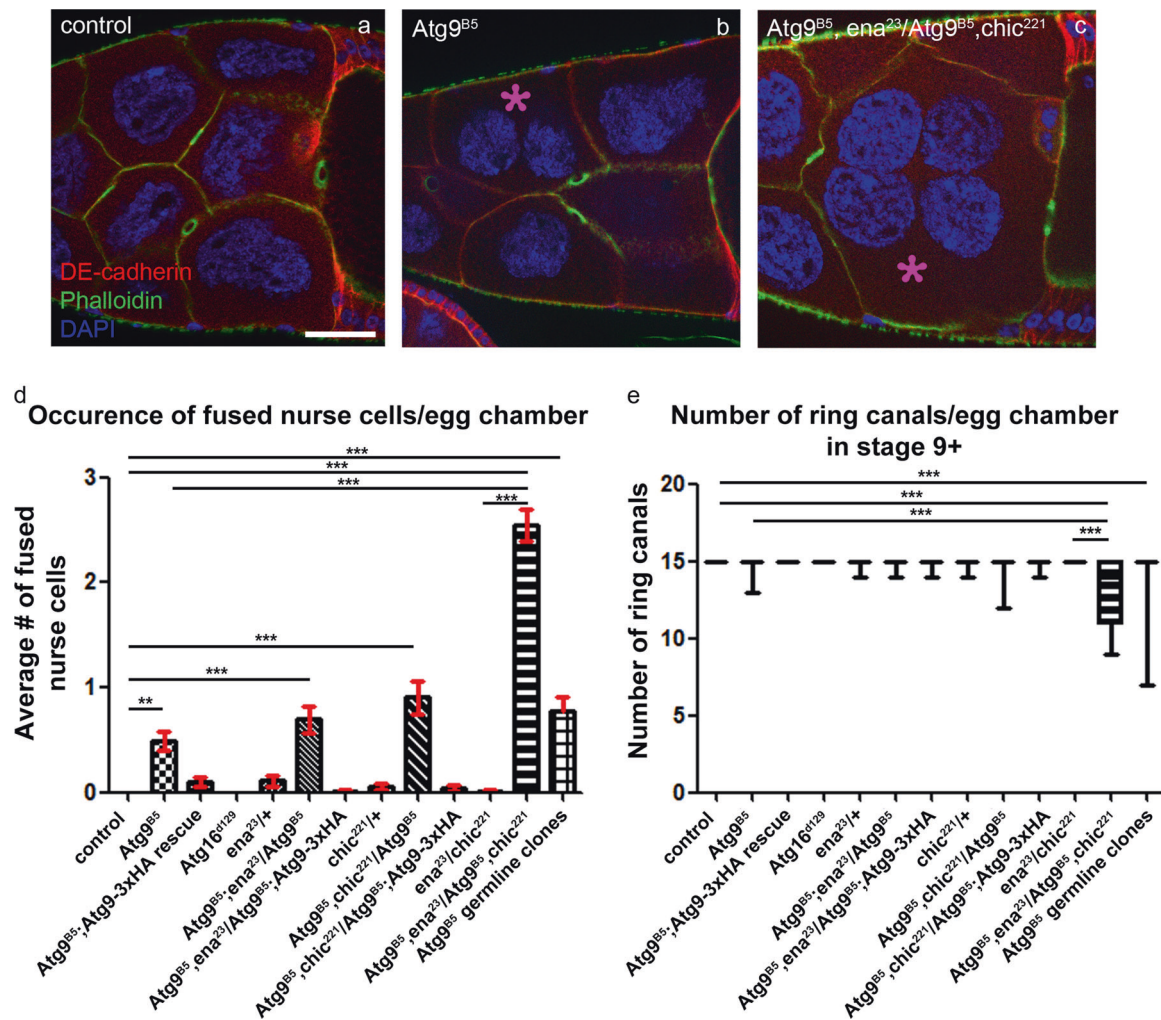
Fig. 4 Atg9 interacts with profilin and Ena/VASP. Cortical actin phalloidin and anti-DE-cadherin immunostaining were used to score the presence of multinucleated nurse cells (marked by asterisks) in stage 9+ egg chambers (**a–d**). This phenotype was never seen in wild type ovaries ($n = 133$, **a**), rarely observed in $Atg9^{B5}$ mutants (131, **b**) and in egg chambers derived from $Atg9^{B5}$ germline clones (149), and became very frequent in homozygous $Atg9^{B5}$ mutants lacking one gene copy of both chic/profilin and Ena, often with the fusion of more than two nurse cells ($n = 231$) (**c**). **d** The statistical evaluation of nurse cell fusions in multiple genotypes including those pictured in **a–c**. Additional genotypes include animals heterozygous for ena^{23} ($n = 92$) or $chic^{221}$ ($n = 124$), double heterozygotes for both genes ($n = 129$), homozygous $Atg16^{d129}$ mutants ($n = 80$), homozygous $Atg9^{B5}$ mutants lacking one functional gene copy of either ena ($n = 150$) or $chic/profilin$ ($n = 97$), Atg9x3HA expressing $Atg9^{B5}$ mutants ($n = 118$) and $Atg9^{B5}$ mutants lacking one functional copy of either ena ($n = 150$) or

$chic/profilin$ ($n = 90$), respectively. Anti-Hts-RC immunostaining was used to score the number of ring canals in stage 9+ egg chambers (**e**). This phenotype was never seen in wild type ovaries ($n = 97$), rarely observed in $Atg9^{B5}$ mutants ($n = 108$) and egg chambers derived from $Atg9^{B5}$ germline clones ($n = 100$), in homozygous $Atg9^{B5}$ mutants lacking one copy of $chic/profilin$ ($n = 67$) or ena ($n = 44$). Double heterozygosity for $chic^{221}$ and $ena^{23\backslash}$ did not affect the number of ring canals ($n = 81$), however, simultaneous lack of one functional copies of both ena and $chic/profilin$ in an $Atg9^{B5}$ mutant background led to very frequent ring canal loss ($n = 34$). Additional genotypes include animals heterozygous for ena^{23} ($n = 93$) or $chic^{221}$ ($n = 94$), homozygous $Atg16^{d129}$ mutants ($n = 88$), Atg9x3HA expressing $Atg9^{B5}$ mutants ($n = 110$), and $Atg9^{B5}$ mutants lacking one copy of either ena ($n = 140$) or $chic/profilin$ ($n = 186$). Statistical analyses were performed using Kruskal–Wallis test, $**p = 0.001$, $***p < 0.001$. Scale bar in panel a represents 50 μm for **a–c**

the appearance of multinucleated, fused NCs with a low frequency (Fig. 4a, b, d). There was a tendency in animals heterozygous for $chic^{221}$ (the gene encoding profilin in *Drosophila*) or ena^{23} in a homozygous *Atg9* mutant background to contain multinuclear NCs more frequently, which became very frequent in the case of heterozygosity for both genes (Fig. 4c, d). Importantly, genomic promoter driven expression of 3xHA-Atg9 readily eliminated NC fusions in

Atg9 mutants (Fig. 4d). NC fusions usually arise as a consequence of impaired actin cytoskeleton integrity, as defects in cortical actin network can destabilize plasma membranes [32]. Importantly, ring canals can be lost after NC fusions, and their numbers in the different genotypes indeed showed largely similar trends as in the case of NC fusions (Fig. 4e). Please note that ring canals freely floating (and often aggregating) in the cytoplasm of NCs were also counted in

these experiments, which explains the differences between NC fusion and ring canal loss data. We also analyzed germline clones to address the germ cell-autonomous role of Atg9, which showed NC fusion and ring canal phenotypes indistinguishable from full-body mutants (Figs. 4d, e, S3a, b).

Heteroallelic combination of profilin mutations (*chic*[221]/ *chic*[01320]) causes fully penetrant sterility with almost no eggs being laid by these hypomorphic mutant females [33]. Of note, germline-specific overexpression of Atg9 on this profilin mutant background did increase the yield of eggs, while Atg9 expression alone did not influence egg laying activity (Fig. S3c, d). Although the deposited eggs were still sterile, this partial rescue supports the in vivo relevance of the interaction of Atg9 and profilin.

To validate the results of our genetic interaction tests, we next performed Y2H experiments. As Atg9 is a multi-spanning membrane protein, we expressed three fragments: the first (CTD1, aa 1–117), second (CTD2, aa 194–334), and fourth (CTD4, aa 530–845) cytosolic domains of Atg9 (the third one is only a few amino acids long) in yeast cells, together with profilin or Ena or Actin itself. There was no detectable interaction between Atg9 fragments and Actin (Fig. 5a). We detected an interaction between CTD1 and Ena (Fig. S4e), and clear binding of CTD4 to profilin, respectively (Fig. 5a). Profilin is known to bind proline-rich motifs with high affinity, so we analyzed the amino acid sequence of CTD4. We have indeed identified a PPRPPAAP sequence in this fragment, which may be responsible for binding profilin. We thus exchanged these prolines to alanines obtaining CTD4 mut_P, which contains the altered motif: AARAAAAA. Y2H experiments revealed that this mutation led to a dramatic reduction of CTD4-

profilin interaction (Fig. 5b). To validate this interaction, we generated a poly-proline binding defective mutant form of profilin. The third amino acid (tryptophan) of human pro-filin was shown to be absolutely critical for binding the proline-rich region of Ena/VASP: changing it to alanine completely eliminated the interaction of these two proteins [34]. This amino acid is conserved from yeast to man, including Drosophila. We thus used a W3A mutant form of profilin for additional Y2H experiments. This mutation not only eliminated the binding of Drosophila profilin to Ena (Fig. S4c, d), but also to CTD4 of Atg9 (Fig. S4a, b).

Finally, recombinant GST-profilin readily pulled down 3xHA-tagged Atg9 from *Drosophila* lysate (Fig. 5c), and FLAG-tagged profilin co-immunoprecipitated Atg9-GFP from fly lysates (Fig. S4f). These data together suggest that Atg9 interacts with the actin regulators profilin and Ena/VASP.

Atg9 colocalizes with and promotes proper Ena and Profilin localization

The genetic and biochemical interactions of Ena and its known binding partner profilin with Atg9 suggested that these proteins all function together in actin cytoskeleton regulation. Indeed, we found that Atg9-GFP and Ena-mCherry structures were frequently adjacent to each other and often showed an overlap, especially along the plasma membrane of NCs (Fig. 6a). Interestingly, their localization is quite intimate in larval salivary gland cells, too: Ena-mCherry positive dots at the cell periphery were almost always surrounded by "nests" of GFP-Atg9 and actin phalloidin staining, sometimes showing partial overlap (Fig. 6b, c). Since profilin showed a predominantly diffuse

Fig. 5 Atg9 binds to profilin. In Y2H assay, Atg9 did not show binding to Actin 5 C, while a strong interaction was detected between the CTD4 (cytosolic domain 4) fragment of Atg9 and profilin (a). A clear reduction in the strength of this interaction was seen when the putative profilin binding PPRPPAAP motif was mutated to AARAAAAA in CTD4 (b). GST pull-down using recombinant GST-profilin also confirmed its interaction with Atg9-3xHA from *Drosophila* lysate (c)
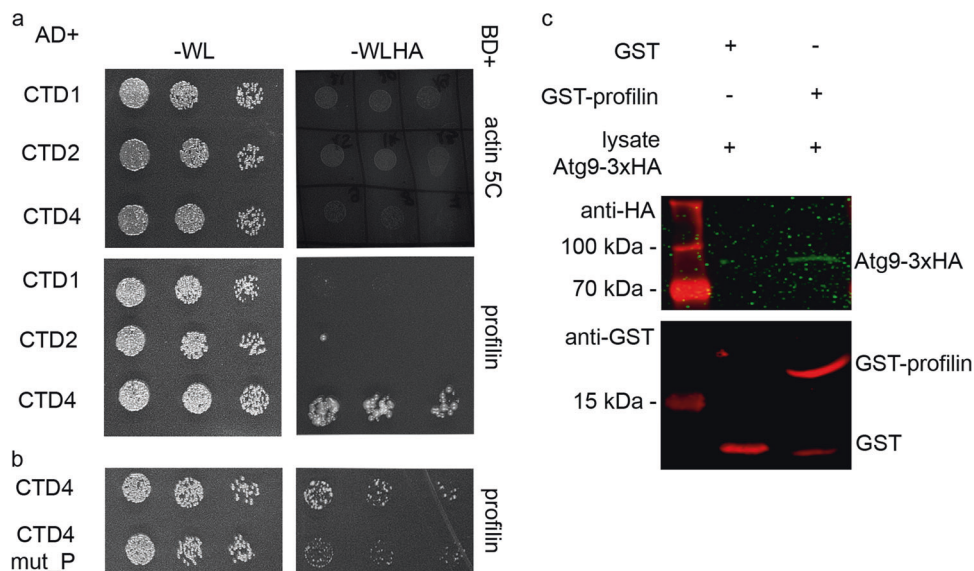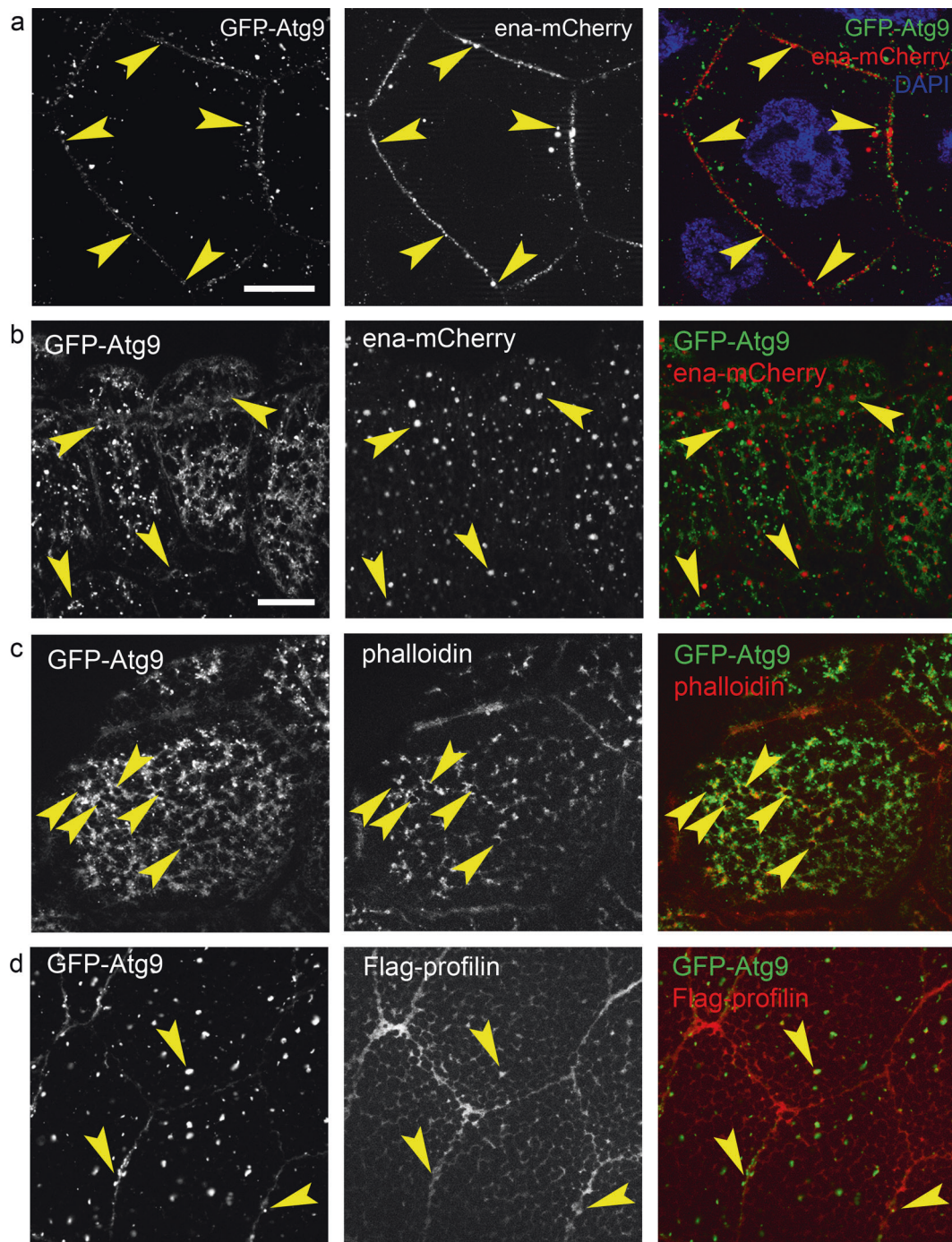
Fig. 6 Colocalization analysis of Atg9, Ena, and profilin. GFP-Atg9 clearly overlaps with Ena-mCherry along the plasma membrane of nurse cells, and these two proteins are adjacent with partial overlap on punctate cytoplasmic structures (arrowheads in **a**). GFP-Atg9 (**b**) and actin phalloidin (**c**) forms ring-like "nests" (arrowheads) around Ena- mCherry positive structures near the periphery of larval salivary gland cells. GFP-Atg9 overlaps with Flag-profilin along the plasma membrane and on cytoplasmic structures (arrowheads) in larval salivary gland cells (**d**). Scale bars represent 20 μm in **a** and **b–d**

cytosolic localization in most tissues including the female germline, we only tested its distribution in salivary gland cells. Structures positive for Atg9 and profilin clearly overlapped with each other, not only at the plasma membrane but also on cytoplasmic puncta (Fig. 6d).

We next visualized the localization of endogenous Ena in wild type and *Atg9* mutant egg chambers. Ena showed a predominantly membrane-associated distribution in wild-type ovaries similar to that seen in case of Atg9 (Fig. 7a, cf. Fig. 3c), and it was also present in ring canals. Strikingly,
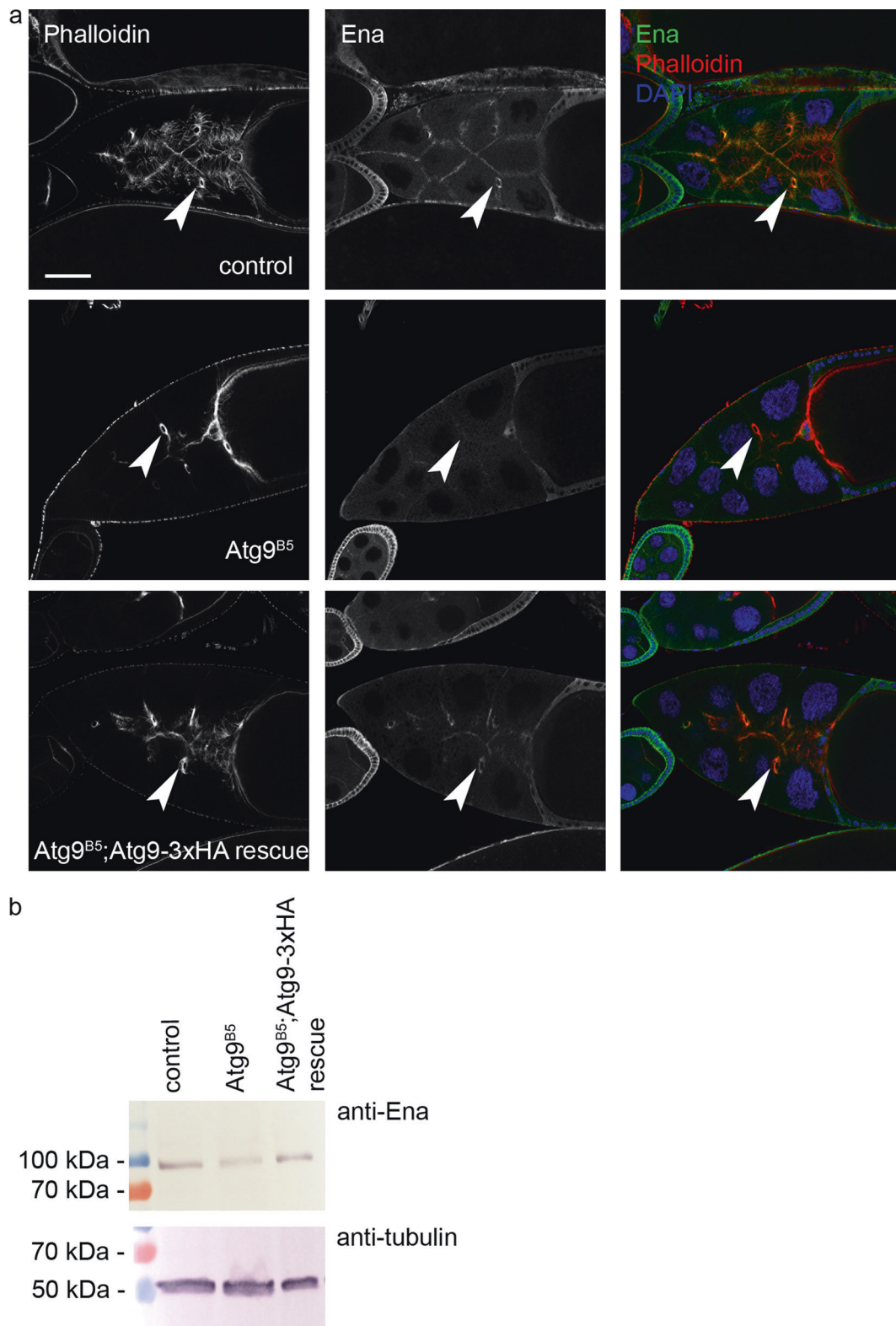
Fig. 7 Atg9 promotes the localization of the actin regulator Ena/VASP. Ablation of Atg9 changes the normally very obvious plasma membrane- and ring canal (arrowheads)-associated distribution of Ena in egg chambers of control and Atg9-3xHA rescued mutant animals (**a**). Decreased level of Ena protein is seen in western blots of Atg9 mutant ovaries compared with control and rescued animals (**b**). Scale bar in **a** represents 50 μm

Fig. 8 Loss of Atg9 increases filopodia number in primary embryonic neurons. Atg9-3xmCherry largely overlaps with actin phalloidin staining at the tip of filopodia (arrowheads), and along the shaft and whole axon in primary embryonic neurons (**a**). Neurons derived from *Atg9* mutant embryos (*n* = 65) have more filopodia when compared with wild type control cells (*n* = 121), *p* = 0.0019, two-tailed two-sample unpaired *t* test (**b**, **c**). Scale bars represent 10 μm in **a** and **b**
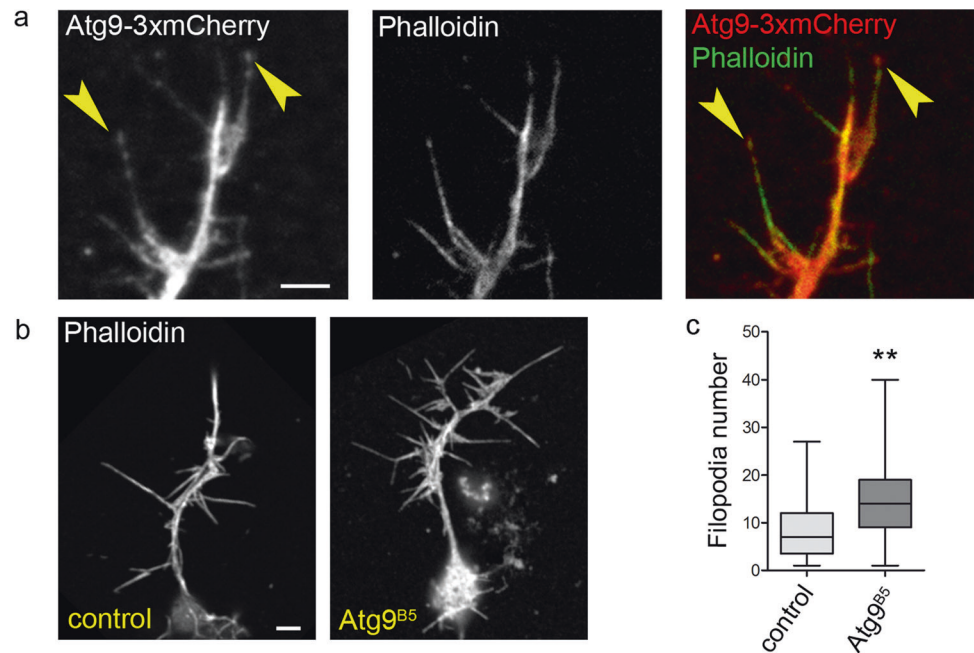
the plasma membrane association of Ena was strongly reduced in *Atg9* mutant egg chambers, which could be rescued by adding back Atg9-3xHA (Fig. 7a). Since the overall level of Ena appeared to decrease based on confocal microscopy, we carried out western blot analysis. Indeed, the level of Ena protein is lower in Atg9 mutant ovaries compared with controls or genetically rescued mutants (Fig. 7b). Thus, Atg9 is required for the proper localization and stability of Ena, in line with their genetic and biochemical interactions.

To test the role of Atg9 in promoting profilin localization, we expressed GFP-Atg9 variants in cultured *Drosophila* cells. The mostly diffuse cytosolic distribution of profilin in control cells (Fig. S5e) changed upon overexpression of GFP-Atg9: endogenous profilin became enriched on GFP+ punctate structures (Fig. S5a). We then overexpressed a GFP-Atg9 variant fused to a KASH (Klarsicht, ANC-1, and Syne Homology) domain responsible for the outer nuclear membrane localization of proteins containing this domain [35]. GFP-Atg9-KASH formed an obvious perinuclear ring, accompanied by a corresponding rim-like perinuclear anti-profilin staining (Fig. S5b). Similarly, we examined the interaction of profilin with the C-terminal part of Atg9. GFP-Atg9C and profilin displayed mostly diffuse cytosolic localization (Fig. S5c), while GFP-Atg9C-KASH targeted to the nuclear membrane again resulted in a corresponding shift of endogenous profilin to the perinuclear region (Fig. S5d). These data confirm that Atg9 plays an important role in the localization of profilin via an interaction that involves its C-terminal cytosolic region.

Atg9 regulates filopodia formation in primary embryonic neurons

Lastly, we turned to another widely used model to study the cytoskeleton: primary embryonic neurons. Both Ena/VASP and profilin are known to play a role in filopodia formation during neurogenesis in *Drosophila* [36]. Importantly, we observed clear overlap of F-actin structures with Atg9–3xmCherry in axons and growth cone filopodia (Fig. 8a), similar to what was seen in case of *Ena*[36]. Interestingly, *Atg9* mutants showed enhanced filopodia formation in primary embryonic neurons compared with controls (Fig. 8b, c), as expected from the lack of this potential actin regulator. It is important to note that we quantified filopodia formation in ex vivo differentiated, isolated neurons, so the alteration seen in *Atg9* mutant cells is likely independent of the proposed role of autophagy in presynaptic assembly [37, 38]. In line with that, *Atg5*[5CC5] autophagy null mutant [21] embryonic neurons showed no change in filopodia numbers relative to controls (Fig. S6d).

Axon growth and pathfinding can be evaluated in vivo in the embryonic central nervous system (CNS), where aberrations are often obvious. The longitudinal non-crossing axon pattern revealed by anti-Fasciclin II staining in wild-type CNS consists of axons running in parallel to the midline in all embryos (Fig. S6a). Interestingly, we observed midline crossing of these axons in a subset of *Atg9* mutant embryos (Fig. S6b). This phenotype was again specific to the loss of Atg9, as *Atg16* autophagy mutants never showed such defects (Fig. S6c). These data suggest that Atg9 also regulates the actin cytoskeleton in neurons,

Discussion

There is increasing evidence that Atg proteins have diverse functions beyond their direct role in autophagosome assembly. Examples include Atg16 function in the intestine to somehow prevent the development of inflammatory bowel disease [39], the role of Atg12 and Atg3 in controlling mitochondrial homeostasis [40], and Atg9 promoting activation of JNK signaling via direct binding to dTRAF6 (tumor necrosis factor receptor-associated factors 6) [28]. More recently, a role for Atg9 was described in antagonizing the activity of Tor kinase, the central positive regulator of cell growth and inhibitor of autophagy [10].

In this work, we uncover an unexpected new role of Atg9 in regulating the actin cytoskeleton. Atg9 likely functions at least in part via binding to the known actin regulators profilin and Ena to regulate their localization. How these proteins promote actin assembly is not entirely clear. Profilin is known to bind to G-actin, and it is thought to deliver monomers to the growing ends of filaments. Ena/VASP has filament bundling and anti-capping activity and enhances filament elongation. Ena is known to bind to profilin as well as G-actin, so a complex of Ena, profilin and actin monomers may be necessary for proper filament elongation [36]. Our work suggests that Atg9 modulates Ena- and profilin-dependent actin filament polymerization via binding to Ena by its CTD1 and profilin by its CTD4, and may restrict the sites and extent of actin assembly near the plasma membrane in nurse cells of the ovary and in embryonic neurons. The appearance of multinucleated nurse cells at a low frequency in *Atg9* mutants and at a much higher frequency in case of halving the dosage of Ena and/or profilin on an *Atg9* mutant genetic background strongly argue for defects in cortical actin integrity. The cortical actin network maintains plasma membranes in the ovary, and its defects likely lead to plasma membrane rupture and the generation of multinucleated nurse cells. These observations suggest that Atg9 is involved in the maintenance of cortical actin integrity in nurse cells, likely via its interactions with profilin and Ena.

Importantly, the stability and proper localization of Ena to the vicinity of nurse cell plasma membranes depends on Atg9. We find that *Drosophila* Atg9 is present in the plasma membrane, similar to mammalian Atg9 [5]. Considering that Atg9 has a tendency to localize to small vesicles and tubules [5, 41], it may cause Atg9 enrichment in highly curved membranes such as actin-rich protrusions in *Drosophila* germ cells, promoting the recruitment and stabilization of Ena. It is important to note that the interaction of profilin with either Ena or Atg9 depends on the same poly-proline binding motif that is disrupted in the W3A mutant form of profilin. While Atg9 could bind to profilin via its CTD4 and to Ena via CTD1 at the same time, we could not show the existence of a stable ternary complex. We thus propose that either this complex is rare/unstable, or Atg9 modulates actin assembly via binding either Ena or profilin but not both at the same time. Such a role for Atg9 is supported by the reduced level and membrane association of Ena in Atg9 mutants.

Importantly, filopodia number is increased in cultured neurons derived from *chic*[221] mutant embryos that lack profilin expression [36], just like in case of *Atg9*[B5] mutant cells. Moreover, CNS defects are observed in <10% of homozygous profilin (*chic*) mutant embryos [23], again resembling *Atg9* null mutant embryonic phenotypes. The actin filament organization defects in nurse cells (including cortical actin and stage 10B bundles), decreased oocyte cytoplasmic streaming, defective border cell migration, and filopodia alterations in neurons all suggest a general role of Atg9 in controlling the actin cytoskeleton in somatic and germ cells. However, the lack of any obvious outer morphological aberrations affecting for example bristle shape and size in Atg9 mutants (which are observed in *chic* transheterozygotes) suggests that this regulation is not universal. Possibly, actin filament assembly is more robust and/or is also regulated by modulators other than Atg9 in these unaffected biological contexts. Future studies of Atg9A and Atg9B double knockout mice should clarify how universal the role of Atg9 is in modulating the actin cytoskeleton.

Regulation of the actin cytoskeleton is thus another function of the transmembrane protein Atg9 in *Drosophila*. Importantly, its CTD4 appears to have multiple interactions: apart from its previously reported binding to TRAFs [28] and the tight junction component Patj and the Tor kinase negative regulator TSC2 [10], we find that it also binds to the actin regulator profilin. How these diverse interactions and regulatory functions of Atg9 are coordinated remains to be established.

Compliance with ethical standards

Conflict of interest The authors declare that they have no conflict of interest.

References

1. Mizushima N, Levine B. Autophagy in mammalian development and differentiation. Nat Cell Biol. 2010;12:823–30.
2. Menzies FM, Fleming A, Caricasole A, Bento CF, Andrews SP, Ashkenazi A, et al. Autophagy and neurodegeneration: pathogenic mechanisms and therapeutic opportunities. Neuron. 2017;93:1015–34.
3. Webber JL, Tooze SA. Coordinated regulation of autophagy by p38alpha MAPK through mAtg9 and p38IP. EMBO J. 2010;29:27–40.
4. Orsi A, Razi M, Dooley H, Robinson D, Weston A, Collinson L, et al. Dynamic and transient interactions of Atg9 with autophagosomes, but not membrane integration, is required for autophagy. Mol Biol Cell. 2012;23:1860–73.
5. Puri C, Renna M, Bento CF, Moreau K, Rubinsztein DC. Diverse autophagosome membrane sources coalesce in recycling endosomes. Cell. 2013;154:1285–99.
6. Barth JM, Hafen E, Kohler K. The lack of autophagy triggers precocious activation of Notch signaling during Drosophila oogenesis. BMC Dev Biol. 2012;12:35.
7. Barth JM, Szabad J, Hafen E, Kohler K. Autophagy in Drosophila ovaries is induced by starvation and is required for oogenesis. Cell Death Differ. 2011;18:915–24.
8. Varga K, Nagy P, Arsikin Csordas K, Kovacs AL, Hegedus K, Juhasz G. Loss of Atg16 delays the alcohol-induced sedation response via regulation of Corazonin neuropeptide production in Drosophila. Sci Rep. 2016;6:34641.
9. Juhasz G, Erdi B, Sass M, Neufeld TP. Atg7-dependent autophagy promotes neuronal health, stress tolerance, and longevity but is dispensable for metamorphosis in Drosophila. Genes Dev. 2007;21:3061–6.
10. Wen JK, Wang YT, Chan CC, Hsieh CW, Liao HM, Hung CC, et al. Atg9 antagonizes TOR signaling to regulate intestinal cell growth and epithelial homeostasis in Drosophila. Elife. 2017;6:1–22.
11. McLean PF, Cooley L. Bridging the divide: illuminating the path of intercellular exchange through ring canals. Fly. 2014;8:13–8.
12. Revenu C, Athman R, Robine S, Louvard D. The co-workers of actin filaments: from cell structures to signals. Nat Rev Mol Cell Biol. 2004;5:635–46.
13. Wear MA, Cooper JA. Capping protein: new insights into mechanism and regulation. Trends Biochem Sci. 2004;29:418–28.
14. Barzik M, Kotova TI, Higgs HN, Hazelwood L, Hanein D, Gertler FB, et al. Ena/VASP proteins enhance actin polymerization in the presence of barbed end capping proteins. J Biol Chem. 2005;280:28653–62.
15. Schirenbeck A, Arasada R, Bretschneider T, Stradal TE, Schleicher M, Faix J. The bundling activity of vasodilator-stimulated phosphoprotein is required for filopodium formation. Proc Natl Acad Sci USA. 2006;103:7694–9.
16. Sechi AS, Wehland J. ENA/VASP proteins: multifunctional regulators of actin cytoskeleton dynamics. Front Biosci: a J virtual Libr. 2004;9:1294–310.
17. Takats S, Glatz G, Szenci G, Boda A, Horvath GV, Hegedus K, et al. Non-canonical role of the SNARE protein Ykt6 in autophagosome-lysosome fusion. PLoS Genet. 2018;14: e1007359.
18. Lorincz P, Lakatos Z, Varga A, Maruzs T, Simon-Vecsei Z, Darula Z, et al. MiniCORVET is a Vps8-containing early endosomal tether in Drosophila. Elife. 2016;5:e14226.
19. Hegedus K, Takats S, Boda A, Jipa A, Nagy P, Varga K, et al. The Ccz1-Mon1-Rab7 module and Rab5 control distinct steps of autophagy. Mol Biol Cell. 2016;27:3132–42.
20. Nagy P, Hegedus K, Pircs K, Varga A, Juhasz G. Different effects of Atg2 and Atg18 mutations on Atg8a and Atg9 trafficking during starvation in Drosophila. FEBS Lett. 2014;588:408–13.
21. Kim M, Sandford E, Gatica D, Qiu Y, Liu X, Zheng Y, et al. Mutation in ATG5 reduces autophagy and leads to ataxia with developmental delay. Elife. 2016;5:1–18.
22. Port F, Chen HM, Lee T, Bullock SL. Optimized CRISPR/Cas tools for efficient germline and somatic genome engineering in Drosophila. Proc Natl Acad Sci USA. 2014;111:E2967–2976.
23. Matusek T, Gombos R, Szecsenyi A, Sanchez-Soriano N, Czibula A, Pataki C, et al. Formin proteins of the DAAM subfamily play a role during axon growth. J Neurosci. 2008;28:13310–9.
24. Kukulski W, Schorb M, Welsch S, Picco A, Kaksonen M, Briggs JA. Precise, correlated fluorescence microscopy and electron tomography of lowicryl sections using fluorescent fiducial markers. Methods Cell Biol. 2012;111:235–57.
25. Szikora S, Földi I, Tóth K, Migh E, Vig A, Bugyi B, et al. The formin DAAM is required for coordination of the actin and microtubule cytoskeleton in axonal growth cones. J Cell Sci. 2017;130:2506–19.
26. Lőrincz P, Tóth S, Benkő P, Lakatos Z, Boda A, Glatz G, et al. Rab2 promotes autophagic and endocytic lysosomal degradation. J Cell Biol. 2017;216:1937–47.
27. Gombos R, Migh E, Antal O, Mukherjee A, Jenny A, Mihály J. The formin DAAM functions as molecular effector of the planar cell polarity pathway during axonal development in Drosophila. J Neurosci. 2015;35:10154–67.
28. Tang HW, Liao HM, Peng WH, Lin HR, Chen CH, Chen GC. Atg9 interacts with dTRAF2/TRAF6 to regulate oxidative stress-induced JNK activation and autophagy induction. Dev Cell. 2013;27:489–503.
29. Pircs K, Nagy P, Varga A, Venkei Z, Erdi B, Hegedus K, et al. Advantages and limitations of different p62-based assays for estimating autophagic activity in Drosophila. PLoS ONE. 2012;7: e44214.
30. Lucas EP, Khanal I, Gaspar P, Fletcher GC, Polesello C, Tapon N, et al. The Hippo pathway polarizes the actin cytoskeleton during collective migration of Drosophila border cells. J Cell Biol. 2013;201:875–85.
31. Gates J, Nowotarski SH, Yin H, Mahaffey JP, Bridges T, Herrera C, et al. Enabled and Capping protein play important roles in shaping cell behavior during Drosophila oogenesis. Dev Biol. 2009;333:90–107.
32. Urwyler O, Cortinas-Elizondo F, Suter B. Drosophila sosie functions with beta(H)-Spectrin and actin organizers in cell migration, epithelial morphogenesis and cortical stability. Biol Open. 2012;1:994–1005.
33. Verheyen EM, Cooley L. Profilin mutations disrupt multiple actin-dependent processes during Drosophila development. Development. 1994;120:717–28.
34. Lambrechts A, Jonckheere V, Dewitte D, Vandekerckhove J, Ampe C. Mutational analysis of human profilin I reveals a second PI(4,5)-P2 binding site neighbouring the poly(L-proline) binding site. BMC Biochem. 2002;3:12.
35. McGee MD, Rillo R, Anderson AS, Starr DA. UNC-83 IS a KASH protein required for nuclear migration and is recruited to the outer nuclear membrane by a physical interaction with the SUN protein UNC-84. Mol Biol Cell. 2006;17:1790–801.
36. Goncalves-Pimentel C, Gombos R, Mihaly J, Sanchez-Soriano N, Prokop A. Dissecting regulatory networks of filopodia formation in a Drosophila growth cone model. PLoS ONE. 2011;6: e18340.

37. Stavoe AK, Hill SE, Hall DH, Colon-Ramos DA. KIF1A/UNC-104 transports ATG-9 to regulate neurodevelopment and autophagy at synapses. Dev Cell. 2016;38:171–85.

38. Shen W, Ganetzky B. Autophagy promotes synapse development in Drosophila. J Cell Biol. 2009;187:71–9.

39. Nagy P, Szatmari Z, Sandor GO, Lippai M, Hegedus K, Juhasz G. Drosophila Atg16 promotes enteroendocrine cell differentiation via regulation of intestinal Slit/Robo signaling. Development. 2017;144:3990–4001.

40. Radoshevich L, Murrow L, Chen N, Fernandez E, Roy S, Fung C, et al. ATG12 conjugation to ATG3 regulates mitochondrial homeostasis and cell death. Cell. 2010;142:590–600.

41. Longatti A, Lamb CA, Razi M, Yoshimura S, Barr FA, Tooze SA. TBC1D14 regulates autophagosome formation via Rab11- and ULK1-positive recycling endosomes. J Cell Biol. 2012;197:659–75.